

Oldroyd-B流体在拉伸板上的Boussinesq近似流动

王雨梦^{ID}

北京建筑大学理学院, 北京

收稿日期: 2026年3月31日; 录用日期: 2026年4月14日; 发布日期: 2026年6月22日

摘要

文章对变本构参数Oldroyd-B流体在非线性拉伸平板上的流动与传热进行了数值模拟。通过引入粘度系数随温度指数的变化,建立了改进的Oldroyd-B流体本构方程。在此基础上,建立了连续性方程、动量方程和能量方程。采用有限差分法对无量纲控制方程进行离散,验证了数值方法的收敛性和准确性。分析了不同雷诺数、普朗特数等关键参数对速度场、温度场和剪应力分布的影响。结果表明,随温度变化的变粘度模型能有效地降低流体中的粘性剪切应力损失。该研究为理解变物性非牛顿流体在拉伸平板条件下的流动与传热机理提供了理论依据,也为相关工业过程的优化设计提供了数值支持。

关键词

Oldroyd-B流体, 变粘度, 拉伸板, 有限差分法

Boussinesq Approximation Flow of Oldroyd-B Fluid on a Stretched Plate

Yumeng Wang^{ID}

School of Science, Beijing University of Civil Engineering and Architecture, Beijing

Received: March 31, 2026; accepted: April 14, 2026; published: June 22, 2026

Abstract

In this paper, the flow and heat transfer of Oldroyd-B fluid with variable constitutive parameters on a nonlinear tensile plate are numerically simulated. The modified Oldroyd-B fluid constitutive equation was established by introducing the change of viscosity coefficient with temperature index. On this basis, the continuity equation, momentum equation, and energy equation are established.

The finite difference method is used to discretize the dimensionless control equation, and the convergence and accuracy of the numerical method are verified. The effects of different Reynolds numbers, Prandtl numbers, and other key parameters on the velocity field, temperature field, and shear stress distribution are analyzed. The results show that the temperature-dependent variable viscosity model can effectively reduce the viscous shear stress loss in the fluid. This study provides a theoretical basis for understanding the flow and heat transfer mechanism of non-Newtonian fluid with variable physical properties under the condition of a stretched plate, and also provides numerical support for the optimization design of related industrial processes.

Keywords

Oldroyd-B Fluid, Variable Viscosity, Stretching Sheet, Finite Difference Method

Copyright © 2026 by author(s) and Hans Publishers Inc.

This work is licensed under the Creative Commons Attribution International License (CC BY 4.0).

<http://creativecommons.org/licenses/by/4.0/>



Open Access

1. 引言

在聚合物挤出、塑料薄膜拉伸、金属板冷却等许多工业制造过程中，流体在拉伸板表面的流动和传热行为直接决定着产品的最终质量和性能。因此，深入研究拉伸板表面流体流动与传热特性不仅具有重要的理论研究价值，还可以为相关工业过程的优化设计提供关键技术支持。

就流体类型而言，早期的研究主要集中在牛顿流体上，而工业上广泛使用的聚合物熔体和润滑剂大多是非牛顿流体，其复杂的流变特性使其流动和传热机理更加特殊。Oldroyd-B 流体作为一种典型的粘弹性非牛顿流体，能够较好地描述流体的弛豫和延迟特性，相关研究逐渐受到关注。Hayat 等人[1]采用同伦分析方法，得到了考虑对流边界条件的 Oldroyd-B 流体边界层流动问题的解析解，并分析了松弛时间、延迟时间等参数对速度和温度分布的影响。Fetecau 和 Kannan [2]研究了剪切应力作用下 Oldroyd-B 流体在平板上的非定常流动，通过 Fourier 余弦变换得到了满足初边值条件的解析解，该解可归结为 Maxwell 流体、二阶流体和 Newton 流体的已知结果。Fetecau 和 Prasad [3]进一步分析了 Oldroyd-B 流体中常加速边引起的流动问题，利用双 Fourier 正弦变换得到了速度场和剪应力的解析表达式，指出当弛豫时间大于延迟时间时，流场会发生振荡。

另外，在实际工程中，存在着非定常流动、局部滑移边界、变厚度拉伸板等复杂工况，这些工况将改变流动与传热的基本规律。Abd El-Aziz [4]修正了非定常拉伸平板流动的相似变换方法，发现在考虑热辐射效应后，增加非定常参数、辐射参数和普朗特数可以提高传热速率；Ariel [5]提出了轴对称部分滑移张力板流的非迭代数值方法和同伦摄动方法，揭示了滑移参数对速度分布和壁面摩擦系数的影响；Fang [6]等人关注了变厚度拉伸板边界层的发展，发现板的非平整度会通过质量吸力或注入效应显著改变边界层厚度和剪应力分布，甚至出现速度超调现象。Liu [7]研究了相对运动半平面驱动 Oldroyd-B 流体的扩展 Stokes 问题，通过积分变换得到了级数形式的速度场解析解。结果表明，弛豫时间和延迟时间对速度演化的影响相反，这为理解复杂边界条件下非牛顿流体的瞬态流动提供了理论依据。

在数值方法方面，Ngondiep [8]提出了一种求解含分数阶导数的二维 Rayleigh-Stokes 问题的高阶有限元方法，适用于加热广义二阶流体的流动和传热分析。该方法具有无条件稳定性和高阶收敛性。Junker 和 Wick [9]提出了一种基于 Hamilton 原理的含内变量非牛顿流体的时空建模方法。将粘度作为一个时空相关的内变量，建立了一个能同时描述剪切变稀和剪切增稠行为的本构模型。Kakati [10]数值研究了微通道

中牛顿流体与牛顿流体、牛顿流体与非牛顿流体组合的热分布对流动的影响，比较了不同微翅片结构下的传热效率，揭示了翅片形状与流体流变性对传热的耦合机理。

现有的研究虽然涵盖了线性和非线性拉伸、牛顿和非牛顿流体、稳态和非稳态流动等多种工况，在传热机理、边界条件等方面取得了许多成果，但仍有进一步拓展的空间。本文通过引入随温度变化的粘滞系数，建立了改进的 Oldroyd-B 流体本构方程，探讨了变本构参数对非线性拉伸板流动与传热的影响。研究发现，考虑温度依赖性的变粘度模型能够更准确地预测流体中的粘性剪切应力和摩擦损失，为后续研究方向的明确和工业应用的实施提供了参考。

2. 模型建立

本章研究的主要内容是非稳态 Oldroyd-B 流体通过半无限拉伸板的流动与传热问题，在动量方程中引入浮力项。假设流动是不可压缩的，并且考虑 Boussinesq 近似。如图 1 所示， x 轴方向与拉伸板平行， y 轴方向垂直于板平面[11]， u 和 v 分别是 x 和 y 方向的速度分量，设平板的非线性拉伸速度为 $u_w = ax^2$ 。

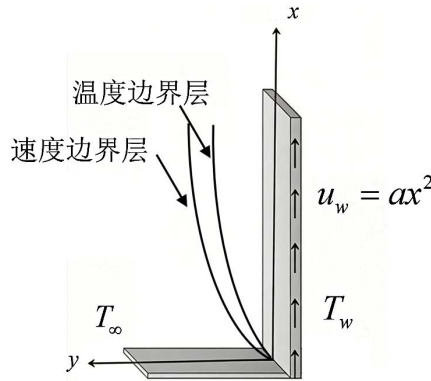


Figure 1. Schematic diagram of the physical model
图 1. 物理模型示意图

Oldroyd-B 流体本构参数随温度的变化：

$$\begin{aligned} \eta_1(T) &= \eta_0 e^{-\alpha T}, \quad \eta_2(T) = \eta_0 \gamma e^{-\beta T}, \\ \lambda_1 &= \frac{\eta_0}{E} (e^{-\alpha T} + \gamma e^{-\beta T}), \quad \lambda_2 = \frac{\eta_0}{E} e^{-\alpha T}. \end{aligned} \tag{1}$$

变粘度 Oldroyd-B 流体的本构方程为：

$$\left[1 + \frac{\eta_0}{E} (e^{-\alpha T} + \gamma e^{-\beta T}) \frac{\partial}{\partial t} \right] S = \eta_0 \gamma e^{-\beta T} \left(1 + \frac{\eta_0}{E} e^{-\alpha T} \frac{\partial}{\partial t} \right) \left(\frac{\partial u}{\partial y} + \frac{\partial v}{\partial x} \right), \tag{2}$$

不可压缩流体的连续性方程、考虑浮力项的动量方程和能量方程为：

$$\frac{\partial u}{\partial x} + \frac{\partial v}{\partial y} = 0, \tag{3}$$

$$\rho_0 \left(\frac{\partial u}{\partial t} + u \frac{\partial u}{\partial x} + v \frac{\partial u}{\partial y} \right) = -\frac{\partial p}{\partial x} + \frac{\partial S}{\partial y} + \rho g, \tag{4}$$

$$\frac{\partial T}{\partial t} + \left(u \frac{\partial}{\partial x} + v \frac{\partial}{\partial y} \right) T = \frac{\kappa}{\rho c_p} \left(\frac{\partial^2}{\partial x^2} + \frac{\partial^2}{\partial y^2} \right) T, \tag{5}$$

其中, $\rho = \rho_0 [1 - \beta_0 (T - T_\infty)]$, Boussinesq 近似仅在浮力项中考虑密度随温度的线性变化[12]。

上述方程的初始条件为:

$$u(x, y, 0) = v(x, y, 0) = 0, T(x, y, 0) = T_\infty. \quad (6)$$

边界条件为:

$$\begin{aligned} u(x, 0, t) &= ax^2, v(x, 0, t) = 0, T(x, 0, t) = T_w, \\ u(x, \infty, t) &= v(x, \infty, t) = 0, T(x, \infty, t) = T_\infty, \end{aligned} \quad (7)$$

其中, a 为拉伸参数, T_w 是在壁面处的温度, T_∞ 是无穷远处的环境温度。

为了简化计算, 将控制方程组、初始条件与边界条件进行无量纲化, 定义以下无量纲量:

$$\begin{aligned} x^* &= \frac{x}{L_0}, y^* = \frac{y}{L_0}, u^* = \frac{ut_0}{L_0}, v^* = \frac{vt_0}{L_0}, t^* = \frac{t}{t_0}, T^* = \frac{T - T_\infty}{T_w - T_\infty}, a^* = at_0 L_0, \\ E^* &= \frac{Et_0}{\eta_0}, g = \frac{g}{a^2 L_0}, p^* = \frac{pt_0^2}{\rho L_0^2}, S^* = \frac{St_0^2}{\rho L_0^2}, \text{Re} = \frac{\rho L_0^2}{t_0 \eta_0}, \rho^* = \frac{\rho}{\rho_0}, \\ \alpha^* &= \alpha \frac{T}{T^*}, \beta^* = \beta \frac{T}{T^*}, \beta_0^* = \beta_0 \frac{T - T_\infty}{T^*} = \beta_0 (T_w - T_\infty), \text{Pr} = \frac{\rho c_p L_0^2}{t_0 \kappa}, \end{aligned} \quad (8)$$

式中, L_0 、 Re 和 Pr 分别是特征长度、雷诺数和普朗特数。

将上述无量纲量(8)代入控制方程组(1)、(3)~(5), 并且忽略无量纲标记“*”, 得到无量纲方程组:

$$\left(1 + \frac{e^{-\alpha T} + \gamma e^{-\beta T}}{E} \frac{\partial}{\partial t}\right) S = \frac{\gamma e^{-\beta T}}{\text{Re}} \left(1 + \frac{e^{-\alpha T}}{E} \frac{\partial}{\partial t}\right) \left(\frac{\partial u}{\partial y} + \frac{\partial v}{\partial x}\right), \quad (9)$$

$$\frac{\partial u}{\partial x} + \frac{\partial v}{\partial y} = 0, \quad (10)$$

$$\frac{\partial u}{\partial t} + u \frac{\partial u}{\partial x} + v \frac{\partial u}{\partial y} = -\frac{\partial p}{\partial x} + \frac{\partial S}{\partial y} + (1 - \beta_0 T) g, \quad (11)$$

$$\frac{\partial T}{\partial t} + \left(u \frac{\partial}{\partial x} + v \frac{\partial}{\partial y}\right) T = \frac{1}{\text{Pr}} \left(\frac{\partial^2}{\partial x^2} + \frac{\partial^2}{\partial y^2}\right) T. \quad (12)$$

无量纲初始条件和边界条件为:

$$\begin{aligned} u(x, y, 0) &= v(x, y, 0) = 0, T(x, y, 0) = 0, \\ u(x, 0, t) &= ax^2, v(x, 0, t) = 0, T(x, 0, t) = 1, \\ u(x, \infty, t) &= v(x, \infty, t) = 0, T(x, \infty, t) = 0. \end{aligned} \quad (13)$$

3. 数值求解

3.1. 有限差分法

控制方程的一阶导数和二阶导数分别采用向后差分格式和中心差分格式进行离散化, 得到无量纲控制方程组:

$$\begin{aligned} & \frac{S_{i,j}^k + S_{i,j}^{k-1}}{2} + \left(e^{-\alpha^* \frac{T_{i,j}^k + T_{i,j}^{k-1}}{2}} + \gamma e^{-\beta^* \frac{T_{i,j}^k + T_{i,j}^{k-1}}{2}} \right) \frac{S_{i,j}^k - S_{i,j}^{k-1}}{E^* \Delta t} \\ &= \frac{\gamma}{\text{Re}} e^{-\beta^* \frac{T_{i,j}^k + T_{i,j}^{k-1}}{2}} \left(\frac{u_{i,j}^k - u_{i,j-1}^k}{\Delta y} + \frac{v_{i,j}^k - v_{i-1,j}^k}{\Delta x} \right) \\ &+ \frac{\gamma}{\text{Re}} e^{-\beta^* \frac{T_{i,j}^k + T_{i,j}^{k-1}}{2}} e^{-\alpha^* \frac{T_{i,j}^k + T_{i,j}^{k-1}}{2}} \frac{u_{i,j}^k - u_{i,j-1}^k - u_{i,j}^{k-1} + u_{i,j-1}^{k-1}}{E^* \Delta t \Delta y} \\ &+ \frac{\gamma}{\text{Re}} e^{-\beta^* \frac{T_{i,j}^k + T_{i,j}^{k-1}}{2}} e^{-\alpha^* \frac{T_{i,j}^k + T_{i,j}^{k-1}}{2}} \frac{v_{i,j}^k - v_{i-1,j}^k - v_{i,j}^{k-1} + v_{i-1,j}^{k-1}}{E^* \Delta t \Delta x}, \end{aligned} \tag{14}$$

$$\begin{aligned} & \frac{T_{i,j}^k}{\Delta t} + \frac{u_{i,j}^k + u_{i,j}^{k-1}}{4\Delta x} T_{i,j}^k + \frac{v_{i,j}^k + v_{i,j}^{k-1}}{4\Delta y} T_{i,j}^k \\ &= \frac{T_{i,j}^{k-1}}{\Delta t} + \frac{u_{i,j}^k + u_{i,j}^{k-1}}{4\Delta x} (T_{i-1,j}^k - T_{i,j}^{k-1} + T_{i-1,j}^{k-1}) + \frac{T_{i,j}^k - 2T_{i-1,j}^k + T_{i-2,j}^k}{2\text{Pr} \Delta x^2} + \frac{T_{i,j}^{k-1} - 2T_{i-1,j}^{k-1} + T_{i-2,j}^{k-1}}{2\text{Pr} \Delta x^2} \\ &+ \frac{v_{i,j}^k + v_{i,j}^{k-1}}{4\Delta y} (T_{i,j-1}^k - T_{i,j}^{k-1} + T_{i,j-1}^{k-1}) + \frac{T_{i,j}^k - 2T_{i,j-1}^k + T_{i,j-2}^k}{2\text{Pr} \Delta y^2} + \frac{T_{i,j}^{k-1} - 2T_{i,j-1}^{k-1} + T_{i,j-2}^{k-1}}{2\text{Pr} \Delta y^2}. \end{aligned} \tag{15}$$

$$\begin{aligned} & \frac{u_{i,j}^k + u_{i,j}^{k-1}}{2} \frac{u_{i,j}^k - u_{i-1,j}^k + u_{i,j}^{k-1} - u_{i-1,j}^{k-1}}{2\Delta x} + \frac{v_{i,j}^k + v_{i,j}^{k-1}}{2} \frac{u_{i,j}^k - u_{i,j-1}^k + u_{i,j}^{k-1} - u_{i,j-1}^{k-1}}{2\Delta y} + \frac{u_{i,j}^k - u_{i,j}^{k-1}}{\Delta t} \\ &= -p_0 + \frac{S_{i,j}^k - S_{i,j-1}^k + S_{i,j}^{k-1} - S_{i,j-1}^{k-1}}{2\Delta y} + \left(1 - \beta_0 \frac{T_{i,j}^k + T_{i,j}^{k-1}}{2} \right) g, \end{aligned} \tag{16}$$

$$\frac{\partial T}{\partial t} + \left(u \frac{\partial}{\partial x} + v \frac{\partial}{\partial y} \right) T = \frac{1}{\text{Pr}} \left(\frac{\partial^2}{\partial x^2} + \frac{\partial^2}{\partial y^2} \right) T. \tag{17}$$

初始条件和边界条件的离散格式为：

$$\begin{aligned} u_{i,j}^0 &= u_{i,j}^1 = 0, v_{i,j}^0 = v_{i,j}^1 = 0, T_{i,j}^0 = T_{i,j}^1 = 0, T_{i,0}^k = 1, \\ u_{i,0}^k &= a(ih_x)^2, v_{i,0}^k = 0, u_{i,M_y}^k = 0, v_{i,M_y}^k = 0, T_{i,M_y}^k = 0. \end{aligned} \tag{18}$$

采用 MATLAB 编程，对控制方程组的离散格式(14)~(17)结合初始条件和边界条件(18)进行求解。

3.2. 收敛性验证

在控制方程组中分别引入源项 $f_1(x, y, t)$ 、 $f_2(x, y, t)$ 和 $f_3(x, y, t)$ [13]，如下所示：

$$\begin{cases} \left(1 + \frac{e^{-\alpha t} + \gamma e^{-\beta t}}{E} \frac{\partial}{\partial t} \right) S = \frac{\gamma e^{-\beta t}}{\text{Re}} \left(1 + \frac{e^{-\alpha t}}{E} \frac{\partial}{\partial t} \right) \left(\frac{\partial u}{\partial y} + \frac{\partial v}{\partial x} \right) + f_1(x, y, t), \\ \frac{\partial u}{\partial x} + \frac{\partial v}{\partial y} = 0, \frac{\partial u}{\partial t} + u \frac{\partial u}{\partial x} + v \frac{\partial u}{\partial y} = -\frac{\partial p}{\partial x} + \frac{\partial S}{\partial y} + (1 - \beta_0 T) g + f_2(x, y, t), \\ \frac{\partial T}{\partial t} + \left(u \frac{\partial}{\partial x} + v \frac{\partial}{\partial y} \right) T = \frac{1}{\text{Pr}} \left(\frac{\partial^2}{\partial x^2} + \frac{\partial^2}{\partial y^2} \right) T + f_3(x, y, t), \end{cases} \tag{19}$$

$$\begin{aligned}
u(x, y, 0) &= 0, v(x, y, 0) = 0, T(x, y, 0) = 0, \\
u(x, 0, t) &= 0, u(x, 3, t) = 0, u(0, y, t) = 0, u(10, y, t) = 0, \\
v(x, 0, t) &= 0, v(x, 3, t) = 0, v(0, y, t) = 0, v(10, y, t) = 0, \\
T(x, 0, t) &= 0, T(x, 3, t) = 0, T(0, y, t) = 0, T(10, y, t) = 0, \\
t \geq 0, 0 &\leq x \leq 10, 0 \leq y \leq 3,
\end{aligned} \tag{20}$$

其中,

$$\begin{aligned}
f_1(x, y, t) &= 5(y-3)x^2t^2 + \frac{10t}{E}(y-3)x^2 \left(e^{-\alpha(3-y)(10-x)xyt^2} + \gamma e^{-\beta(3-y)(10-x)xyt^2} \right) \\
&+ \frac{\gamma}{\text{Re}} e^{-\beta(3-y)(10-x)xyt^2} \left(3(10-x)x(2y-3)t^2 + (2y-9)y^2t^2 \right) \\
&+ \frac{\gamma}{\text{Re}E} e^{-(\beta+\alpha)(3-y)(10-x)xyt^2} \left(6(10-x)x(2y-3)t + 2(2y-9)y^2t \right),
\end{aligned} \tag{21}$$

$$\begin{aligned}
f_2(x, y, t) &= 6(3-y)(10-x)xyt + 18(10-x)x(3-y)^2(5-x)y^2t^4 + \frac{\partial p}{\partial x} - 5x^2t^2 \\
&+ 3(9-2y)(x-5)y^2(3-2y)(10-x)xt^4 - g + \beta_0 g(3-y)(10-x)xyt^2,
\end{aligned} \tag{22}$$

$$\begin{aligned}
f_3(x, y, t) &= 2t(3-y)(10-x)xy + (9-2y)(x-5)y^2(3-2y)(10-x)xt^4 \\
&+ 6(10-x)x(3-y)^2(5-x)y^2t^4 + \frac{2t^2}{\text{Pr}}(3y-y^2+10x-x^2),
\end{aligned} \tag{23}$$

方程(19)和(20)的精确解如下:

$$\begin{aligned}
\bar{u}(x, y, t) &= 3(3-y)(10-x)xyt^2, \bar{v}(x, y, t) = (9-2y)(x-5)y^2t^2, \\
\bar{T}(x, y, t) &= (3-y)(10-x)xyt^2, S(x, y, t) = 5(y-3)x^2t^2.
\end{aligned} \tag{24}$$

含有源项的控制方程组的差分格式如下:

$$\begin{aligned}
&\frac{S_{i,j}^k + S_{i,j}^{k-1}}{2} + \left(e^{-\alpha \frac{T_{i,j}^k + T_{i,j}^{k-1}}{2}} + \gamma e^{-\beta \frac{T_{i,j}^k + T_{i,j}^{k-1}}{2}} \right) \frac{S_{i,j}^k - S_{i,j}^{k-1}}{E^* \Delta t} \\
&= \frac{\gamma}{\text{Re}} e^{-\beta \frac{T_{i,j}^k + T_{i,j}^{k-1}}{2}} \left(\frac{u_{i,j}^k - u_{i,j-1}^k}{\Delta y} + \frac{v_{i,j}^k - v_{i-1,j}^k}{\Delta x} \right)
\end{aligned} \tag{25}$$

$$\begin{aligned}
&+ \frac{\gamma}{\text{Re}} e^{-\beta \frac{T_{i,j}^k + T_{i,j}^{k-1}}{2}} e^{-\alpha \frac{T_{i,j}^k + T_{i,j}^{k-1}}{2}} \frac{u_{i,j}^k - u_{i,j-1}^k - u_{i,j}^{k-1} + u_{i,j-1}^{k-1}}{E^* \Delta t \Delta y} \\
&+ \frac{\gamma}{\text{Re}} e^{-\beta \frac{T_{i,j}^k + T_{i,j}^{k-1}}{2}} e^{-\alpha \frac{T_{i,j}^k + T_{i,j}^{k-1}}{2}} \frac{v_{i,j}^k - v_{i-1,j}^k - v_{i,j}^{k-1} + v_{i-1,j}^{k-1}}{E^* \Delta t \Delta x} + f_1(x_i, y_j, t_k), \\
&\frac{u_{i,j}^k - u_{i-1,j}^k + u_{i,j}^{k-1} - u_{i-1,j}^{k-1}}{2\Delta x} + \frac{v_{i,j}^k - v_{i,j-1}^k + v_{i,j}^{k-1} - v_{i,j-1}^{k-1}}{2\Delta y} = 0,
\end{aligned} \tag{26}$$

$$\begin{aligned}
&\frac{u_{i,j}^k - u_{i,j}^{k-1}}{\Delta t} + \frac{u_{i,j}^k + u_{i,j}^{k-1}}{2} \frac{u_{i,j}^k - u_{i-1,j}^k + u_{i,j}^{k-1} - u_{i-1,j}^{k-1}}{2\Delta x} + \frac{S_{i,j}^k - S_{i,j-1}^k + S_{i,j}^{k-1} - S_{i,j-1}^{k-1}}{2\Delta y} \\
&+ \frac{v_{i,j}^k + v_{i,j}^{k-1}}{2} \frac{u_{i,j}^k - u_{i,j-1}^k + u_{i,j}^{k-1} - u_{i,j-1}^{k-1}}{2\Delta y} = -p_0 + \left(1 - \beta_0 \frac{T_{i,j}^k + T_{i,j}^{k-1}}{2} \right) g + f_2(x_i, y_j, t_k),
\end{aligned} \tag{27}$$

$$\begin{aligned}
 & \frac{T_{i,j}^k}{\Delta t} + \frac{u_{i,j}^k + u_{i,j}^{k-1}}{4\Delta x} T_{i,j}^k + \frac{v_{i,j}^k + v_{i,j}^{k-1}}{4\Delta y} T_{i,j}^k \\
 &= \frac{T_{i,j}^{k-1}}{\Delta t} + f_3(x_i, y_j, t_k) + \frac{u_{i,j}^k + u_{i,j}^{k-1}}{4\Delta x} (T_{i-1,j}^k - T_{i,j}^{k-1} + T_{i-1,j}^{k-1}) + \frac{T_{i,j}^k - 2T_{i-1,j}^k + T_{i-2,j}^k}{2\text{Pr}\Delta x^2} + \frac{T_{i,j}^{k-1} - 2T_{i-1,j}^{k-1} + T_{i-2,j}^{k-1}}{2\text{Pr}\Delta x^2} \\
 & \quad + \frac{v_{i,j}^k + v_{i,j}^{k-1}}{4\Delta y} (T_{i,j-1}^k - T_{i,j}^{k-1} + T_{i,j-1}^{k-1}) + \frac{T_{i,j}^k - 2T_{i,j-1}^k + T_{i,j-2}^k}{2\text{Pr}\Delta y^2} + \frac{T_{i,j}^{k-1} - 2T_{i,j-1}^{k-1} + T_{i,j-2}^{k-1}}{2\text{Pr}\Delta y^2}.
 \end{aligned} \tag{28}$$

初始条件和边界条件的离散格式为:

$$\begin{aligned}
 & u_{i,j}^0 = u_{i,j}^1 = 0, v_{i,j}^0 = v_{i,j}^1 = 0, T_{i,j}^0 = T_{i,j}^1 = 0, \\
 & u_{0,j}^k = 0, u_{M_x,j}^k = 0, v_{0,j}^k = 0, v_{M_x,j}^k = 0, T_{0,j}^k = 0, T_{M_x,j}^k = 0, \\
 & u_{i,0}^k = 0, u_{i,M_y}^k = 0, v_{i,0}^k = 0, v_{i,M_y}^k = 0, T_{i,0}^k = 0, T_{i,M_y}^k = 0.
 \end{aligned} \tag{29}$$

当设置参数为 $\text{Re} = 50$ 、 $\text{Pr} = 5$ 、 $\alpha = 5$ 、 $\beta = 4$ 和 $\gamma = 8$ 时，选取计算域的中间剖面 $y = 1.5$ ，数值解与解析解的比较曲线如图 2 所示。代表数值解的散点与代表解析解的曲线拟合良好，验证了数值方法的准确性。

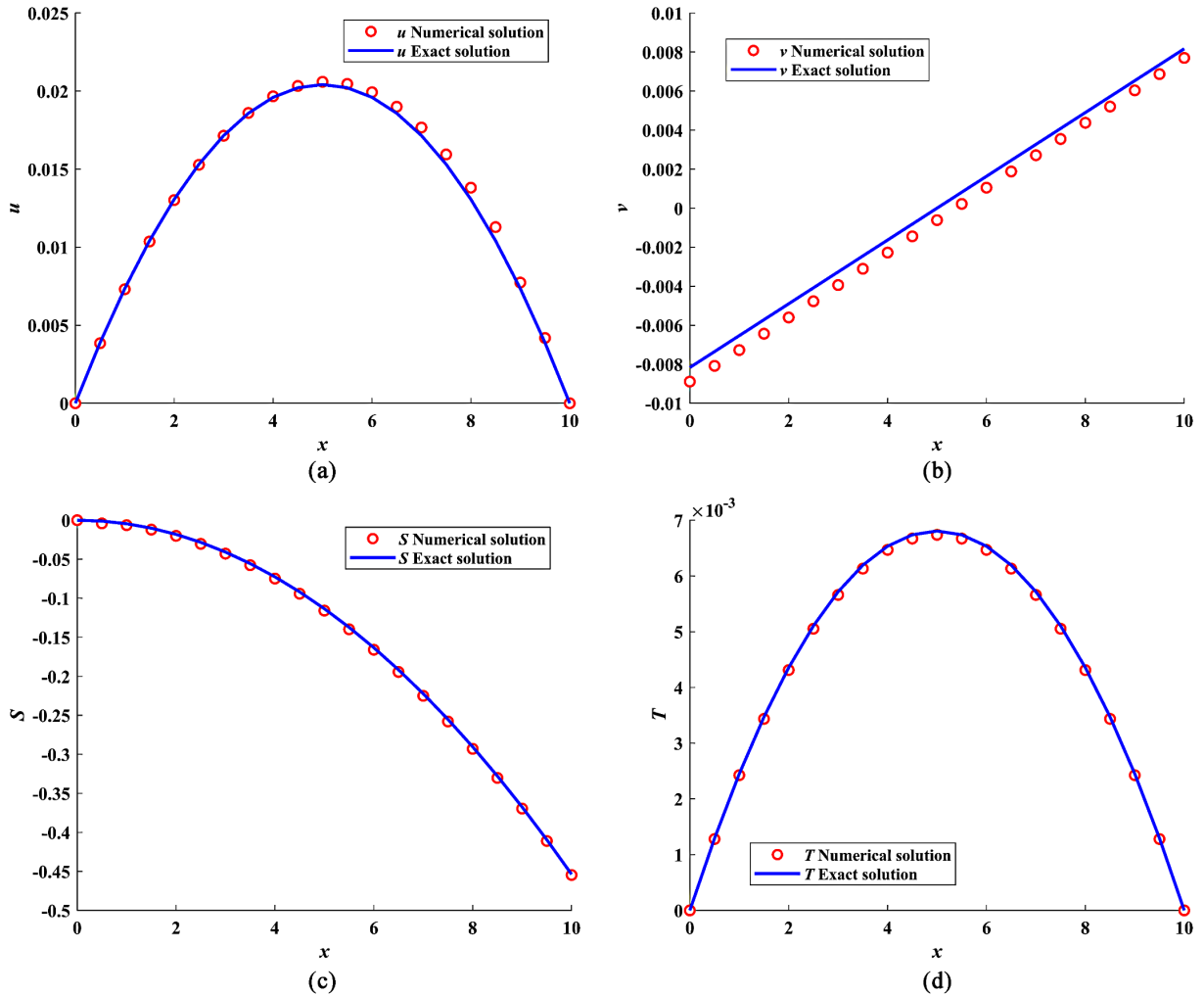


Figure 2. Comparison between numerical solution and exact solution ($y = 1.5$)
 图 2. 数值解和精确解的比较($y = 1.5$)

4. 结果与讨论

通过有限差分法进行数值模拟，计算得到 Oldroyd-B 流体在拉伸板上的 Boussinesq 近似流动。图 3~5 展示了雷诺数 Re 和普朗特数 Pr 对流体流动的影响。

从图 3 给出的速度分布曲线可以发现，流速 u 随着雷诺数 Re 的增大而呈现下降趋势。这种现象的物理本质在于雷诺数表征了流体惯性力与粘性力的相对比值。当 Re 提升时，流体的惯性作用增强，在特定的边界条件或收缩区域内，这种增强的惯性效应会导致速度梯度分布发生改变，使得流体在相同位置处的动量表现有所减弱，进而导致流速减慢。

随着 Re 增大，惯性效应占据主导，粘性对流动的约束作用减弱，动量边界层厚度被压缩，壁面速度梯度显著降低，流体在近壁区域的速度衰减速率加快，进而使整体流速呈现下降趋势。同时，壁面速度梯度的减小直接削弱了流体层间的相对滑移强度，为剪切应力的降低提供了动力学基础。

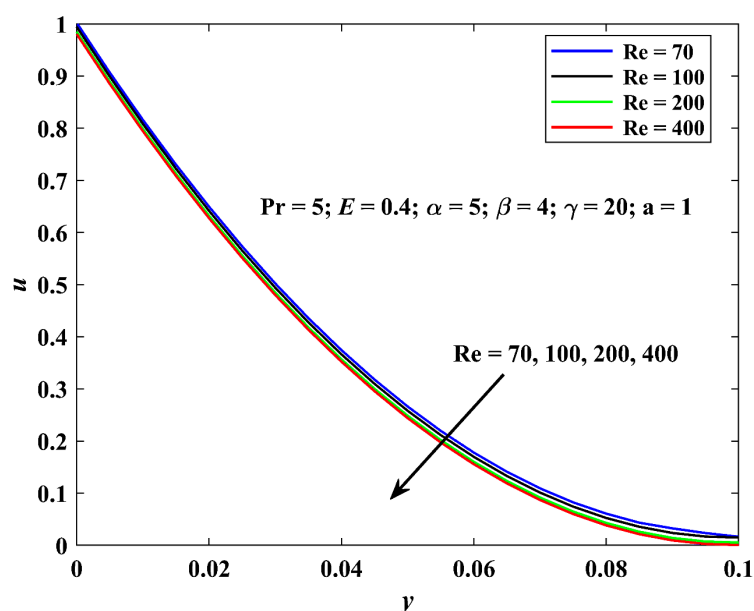


Figure 3. Effect of Reynolds number on velocity distribution ($Re = 70, 100, 200, 400$)

图 3. 雷诺数对速度分布的影响($Re = 70, 100, 200, 400$)

图 4 刻画了普朗特数 Pr 对流体温度场的影响规律。观察可见，随着 Pr 值的增加，流体温度 T 出现了显著的衰减。从热对流机理来看，普朗特数是动量扩散率与热扩散率之比。较高的普朗特数意味着流体的热传导能力相对其运动粘性较弱，这限制了热量从壁面，向流体内部的传递效率。因此，随着 Pr 的增大，热边界层变薄，流体区域内的整体温度水平也随之降低。

Pr 增大时，流体动量扩散能力远强于热扩散能力，热边界层厚度大幅缩减，热量难以从壁面向流体主体传递，导致近壁温度梯度急剧增大，远壁温度快速趋近环境温度。这种温度梯度的分布变化，不仅改变了能量运输效率，更通过温度与粘度的耦合关系，间接影响流场内部的粘性作用强度。

通过对控制方程组(14)~(17)进行数值模拟求解，得到剪切应力 S 的分布情况，由图 5 可知，雷诺数 Re 的增大导致了剪切应力向数值增加的方向移动，负值的绝对值减小。雷诺数的提高反映了粘性力对流动阻碍作用的相对减弱。随着惯性力主导地位的提升，流体层间的摩擦阻力效应受到抑制，使得剪切应力 S 的分布曲线随 Re 的增加而上升。这种变化趋势说明，提高雷诺数有利于减小流体内部的粘性摩擦损耗。

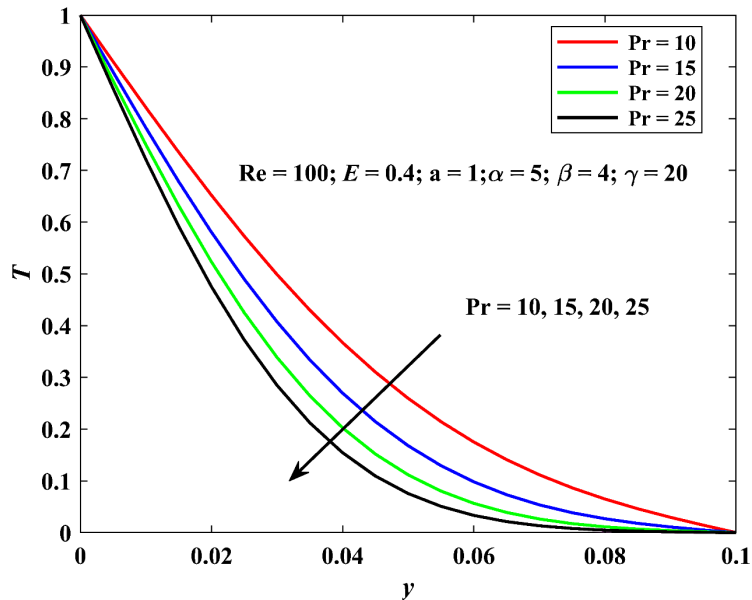


Figure 4. Effects of Prandtl number on temperature (Pr = 10, 15, 20, 25)
图 4. 普朗特数对温度变化的影响(Pr = 10, 15, 20, 25)

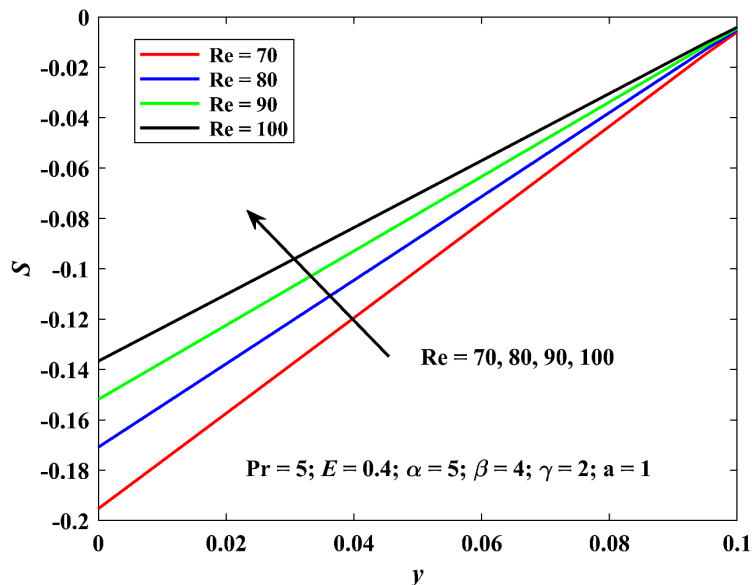


Figure 5. Effects of Reynolds number on shear stress distribution (Re = 70, 80, 90, 100)
图 5. 雷诺数对剪切应力分布的影响(Re = 70, 80, 90, 100)

本文所采用的变粘度 Oldroyd-B 模型中，温度场与流场存在双向耦合作用：一方面，流场的速度分布与剪切作用决定流体内部的粘性耗散强度，直接影响温度场的生成与扩散，流速与剪切应力越大，粘性耗散越强，流体局部温度越高；另一方面，温度场通过变粘度本构关系反向调控流场动力学特性，温度升高会使流体粘度呈指数规律变化，改变粘性力对流动的约束效果，进而修正速度分布与剪切应力分布。

5. 总结

本文从理论上探讨了 Oldroyd-B 流体在拉伸板上的不可压缩流动及传热问题，借助有限差分法对控

制方程组进行了数值求解。通过对模拟结果的详细分析，得出以下主要结论：雷诺数对流场的演化具有显著影响，随着雷诺数的增大，收缩区域内的流体速度呈现明显的减小趋势；同时，增大雷诺数会导致剪切应力的绝对值减小。这揭示了在收缩通道中，惯性力与粘性力的相对强弱变化是调控流体动量运输的关键因素。普朗特数是决定温度场分布的核心参数，流体温度随普朗特数的增加而显著降低。这说明通过改变流体物理性质，如扩散能力比值，可以有效控制收缩通道内的热量渗透深度和热边界层厚度。Pr 增大带来的高动量扩散率会使速度边界层变薄，壁面速度梯度减小，二者共同作用下，流体层间的剪切作用被削弱，剪切应力负值绝对值降低。而当 Pr 较小时，热扩散能力增强，温度边界层扩张，流体整体温度升高，粘度降低，粘性阻力减弱，理论上剪切应力会进一步减小，但低速扩散率使速度梯度增大，抵消了部分低粘度效应，最终使剪切应力维持在较高水平。这一过程清晰表明：普朗特数通过改变温度场分布，调控流体粘度，再经由粘度 - 动量耦合关系，充分体现了变物性非牛顿流体中热参数与动力学参数的强耦合特性。研究表明，通过合理调节雷诺数、普朗特数等物理参数，能够实现 Oldroyd-B 流体流速、温度分布及壁面剪切力的精准调控。这些规律深入揭示了非牛顿流体的动力学演化机制，为相关控制设备的设计、优化以及流体热管理技术的应用提供了重要的科学依据和理论指导。

参考文献

- [1] Hayat, T., Awais, M. and Obaidat, S. (2012) Similar Solution for Three-Dimensional Flow in an Oldroyd-B Fluid over a Stretching Surface. *International Journal for Numerical Methods in Fluids*, **70**, 851-859. <https://doi.org/10.1002/flid.2716>
- [2] Fetecau, C. and Kannan, K. (2005) A Note on an Unsteady Flow of an Oldroyd-B Fluid. *International Journal of Mathematics and Mathematical Sciences*, **2005**, 3185-3194. <https://doi.org/10.1155/ijmms.2005.3185>
- [3] Fetecau, C. and Prasad, S.C. (2005) A Note on the Flow Induced by a Constantly Accelerating Edge in Anoldroyd-B Fluid. *International Journal of Mathematics and Mathematical Sciences*, **2005**, 2677-2688. <https://doi.org/10.1155/ijmms.2005.2677>
- [4] Abd El-Aziz, M. (2009) Radiation Effect on the Flow and Heat Transfer over an Unsteady Stretching Sheet. *International Communications in Heat and Mass Transfer*, **36**, 521-524. <https://doi.org/10.1016/j.icheatmasstransfer.2009.01.016>
- [5] Ariel, P.D. (2007) Axisymmetric Flow Due to a Stretching Sheet with Partial Slip. *Computers & Mathematics with Applications*, **54**, 1169-1183. <https://doi.org/10.1016/j.camwa.2006.12.063>
- [6] Fang, T., Zhang, J. and Zhong, Y. (2012) Boundary Layer Flow over a Stretching Sheet with Variable Thickness. *Applied Mathematics and Computation*, **218**, 7241-7252. <https://doi.org/10.1016/j.amc.2011.12.094>
- [7] Liu, C.M. (2011) Extended Stokes' First Problem of an Oldroyd-B Fluid for Relatively Moving Half-Planes. *Mathematical Problems in Engineering*, **2011**, Article ID: 709836. <https://doi.org/10.1155/2011/709836>
- [8] Ngondiep, E. (2025) A High-Order Finite Element Method for Solving Two-Dimensional Fractional Rayleigh-Stokes Problem for a Heated Generalized Second Grade Fluid. *International Journal for Numerical Methods in Fluids*, **97**, 605-620. <https://doi.org/10.1002/flid.5361>
- [9] Junker, P. and Wick, T. (2025) Space-Time Modeling and Numerical Simulations of Non-Newtonian Fluids Using Internal Variables. *International Journal for Numerical Methods in Fluids*, **97**, 1457-1481. <https://doi.org/10.1002/flid.5406>
- [10] Kakati, A., Gupta, S., Basu, M. and Bit, A. (2026) Numerical Investigation of the Impact of Heat Distribution on Fluid Flow for the Combination of Newtonian-Newtonian and Newtonian-Non-Newtonian Fluid. *International Journal for Numerical Methods in Fluids*, **98**, 546-556. <https://doi.org/10.1002/flid.70055>
- [11] Hajjaligol, N. (2025) Energy Transition in Bioconvective Darcy-Forchheimer Nanofluid Flow: A Numerical Study. *International Journal of Nano Dimension*, **16**, Article 162518.
- [12] Barletta, A., Celli, M. and Rees, D.A.S. (2023) On the Use and Misuse of the Oberbeck-Boussinesq Approximation. *Physics*, **5**, 298-309. <https://doi.org/10.3390/physics5010022>
- [13] Suleiman, K., Liu, C., Zhang, X., Wang, E., Ma, L. and Zheng, L. (2020) Anomalous Diffusion on Archimedean Spiral Structure with Cattaneo Flux Model. *Journal of Molecular Liquids*, **319**, Article 114256. <https://doi.org/10.1016/j.molliq.2020.114256>